Short-Pulse Propagation in a Hollow Waveguide: Analysis, Optoelectronic Measurement, and Signal Processing

David Kralj, Lin Mei, Teng-Tai Hsu, *Member, IEEE*, and Lawrence Carin, *Member, IEEE*

***Abstract*—An asymptotic analysis is performed for short-pulse propagation in a hollow waveguide. It is demonstrated that each time-domain mode supported by the guide is characterized by a time-dependent frequency which, as time proceeds, approaches the modal cutoff frequency. This phenomenon is demonstrated experimentally by performing short-pulse optoelectronic measurements for the case of rectangular waveguide. In these measurements a short-pulse laser is used to switch planar antennas photoconductively, generating freely propagating waveforms with instantaneous bandwidth from 15–75 GHz. Time-frequency signal processing is performed on the measured data, the results of which are in close agreement with the predictions of the asymptotic analysis.**

I. Introduction

THE EFFECTS of dispersion on time-domain electromagnetic propagation has been the subject of significant interest for many decades [1]–[6]. As is well known, dispersion is caused by the frequency-dependent electrical properties of materials (material dispersion) and by the frequency-dependent effects of a guiding structure (structural dispersion). In this paper we investigate structural dispersion associated with time-domain propagation in a hollow waveguide. This is a basic electromagnetic problem which has been investigated previously [7], [8]. However, most previous studies have considered relatively narrowband waveforms [7], [8]; in the present investigation we concentrate on the propagation of wideband short-pulse signals which excite several time-domain waveguide modes.

Structural dispersion has been investigated theoretically for time-domain Floquet modes excited by a finite periodic [4] or weakly aperiodic [5] grating, time-domain leaky modes supported by a dielectric slab [6], and for time-domain modal propagation in a hollow waveguide [7], [8]. Each of these time-domain modes is characterized by a chirped waveform [4]–[6]. In this paper we analyze short-pulse time-domain propagation in an arbitrary hollow waveguide and present theoretical and experimental results for the particular case of a rectangular waveguide. The time-domain waveguide modes are analyzed using a first-order asymptotic procedure which results in a simple closed-form expression for the time-domain fields; except for very early times, the asymptotic results are in nearly exact agreement with a fast Fourier transform (FFT) of the frequency-domain fields. Further, the asymptotic analysis parametrizes the transient modal fields in terms of time-dependent instantaneous frequencies, thereby explaining the chirped nature of the time-domain waveguide modes as well as providing a tool for predicting the approximate modal turn-on times.

The measurements are performed optoelectronically using an ultra-fast laser to photoconductively switch planar antennas [9]–[11]. The freely propagating short-pulse waveforms have instantaneous bandwidths of 15–75 GHz, allowing a unique opportunity for the investigation of wideband, multi-mode transient propagation in a hollow waveguide. The measured results are processed using a short-time Fourier transform (STFT) [12]–[14], revealing the time-dependent modal dispersion curves in the time-frequency phase space; these dispersion curves are shown to be in good agreement with the predictions of the asymptotic analysis.

The remainder of the text is organized as follows. The asymptotic analysis is outlined in Section II along with a detailed discussion of the implications of the results on short-pulse propagation in a waveguide. Further, in this section we examine the accuracy of the asymptotics for the case of rectangular waveguide. The experimental facility is discussed in Section III along with results for two measurements. The measured time-domain waveforms are processed using a STFT, yielding time-frequency phase-space representations of the data which are compared with the expectations of the asymptotic analysis. Conclusions are discussed in Section IV.

II. Analysis

A. Stationary-Point Asymptotics

Consider the hollow waveguide of arbitrary cross section in Fig. 1. For time-harmonic propagation in the positive z direction the electric field $\mathbf{E}(x, y, z, \omega)$ can be expressed as [15]

$$\mathbf{E}(x, y, z, \omega) = \sum_{k=1}^{\infty} d_k(\omega)\mathbf{e}_k(x, y) \exp[-jk_{zk}(\omega)z] \exp(j\omega t) \tag{1}$$

Manuscript received January 30, 1995; revised May 25, 1995. This work was supported in part by the National Science Foundation Grant ECS-9211353.

D. Kralj, L. Mei, and T.-T. Hsu are with the Department of Electrical Engineering, Polytechnic University, Brooklyn, NY 11201 USA.

L. Carin was with the Department of Electrical Engineering, Polytechnic University, Brooklyn, NY 11201 USA. He is now with the Department of Electrical Engineering, Duke University, Durham, NC 27708 USA.

IEEE Log No. 94134188.

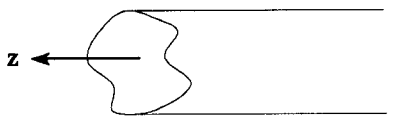

Fig. 1. Hollow waveguide of arbitrary cross section.

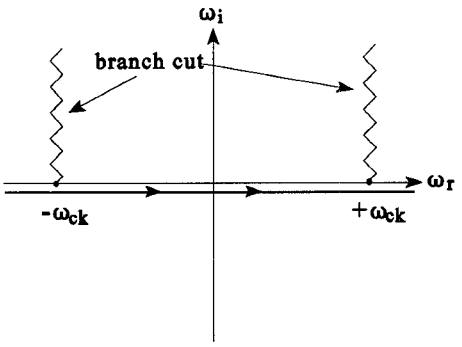

Fig. 2. Integration path in the complex-ω plane for the spectral integral in (3).

where $\mathbf{e}_k(x,y)$ and $d_k(\omega)$ are respectively the modal electric fields and excitation amplitude for the kth waveguide mode. The longitudinal wavenumber is

$$k_{zk} = k_0\sqrt{1-(\omega_{ck}/\omega)^2} \tag{2}$$

where $k_0 = \omega/c$, c is the speed of light in vacuum, and ω_{ck} is the cutoff frequency of the kth waveguide mode. The fields in (1) can be converted to the time domain via a Fourier transform

$$\mathbf{E}(x,y,z,t) = \frac{1}{2\pi}\sum_{k=1}^{\infty}\mathbf{e}_k(x,y) \times \int_{-\infty}^{\infty} d_k(\omega)\exp[j\phi_k(\omega,z,t)]\,d\omega$$
$$\phi_k(\omega,z,t) = \omega t - zk_{zk}(\omega). \tag{3}$$

For causality ($\mathbf{E}(x,y,z,t<z/c)=0$) the path of integration in (3) is slightly below the real-ω axis and the branch cuts emanating from $\omega = \pm\omega_{ck}$ reside in the top half of the complex ω plane (see Fig. 2).

For cases in which the factor $\exp[j\phi_k(\omega,z,t)]$ is highly oscillatory with respect to the amplitude $d_k(\omega)$, the integrals in (3) can be evaluated approximately via stationary-point asymptotics [16]. The stationary-point condition is given as

$$\left.\frac{\partial\phi(\omega,z,t)}{\partial\omega}\right|_{\omega=\omega_{sk}} = 0 \Rightarrow t = z\left.\frac{\partial k_{zk}(\omega)}{\partial\omega}\right|_{\omega=\omega_{sk}}. \tag{4}$$

Recognizing that the frequency-dependent group velocity of the kth mode is given by

$$v_{gk}(\omega) \equiv \left(\frac{\partial k_{zk}(\omega)}{\partial\omega}\right)^{-1} \tag{5}$$

the stationary-point condition in (4) can be expressed as $t = z/v_{gk}(\omega_{sk})$. Therefore the asymptotic analysis indicates that the frequency components which arrive at the observer first have the fastest group velocities, while frequency components with slower group velocities arrive later in time. Using (2) in (4) the stationary-point condition can be expressed explicitly as

$$\omega_{sk}(z,t) = \pm\frac{\omega_{ck}}{\sqrt{1-(z/ct)^2}} \tag{6}$$

demonstrating that the initial frequency components from a given mode are large, and with increasing time the modal instantaneous frequency decreases, eventually approaching the modal cutoff frequency ω_{ck} for $t \gg z/c$. Note that the asymptotic results are invalid for $t \approx z/c$ since the phase

$$\phi_k(\omega,z,t) = \omega\left[t - \frac{z}{c}\sqrt{1-(\omega_{ck}/\omega)^2}\right] \tag{7}$$

vanishes for $\omega \to \omega_{ck}$, violating our original assumption with regard to the use of asymptotics; however, as demonstrated below for the case of rectangular waveguide, the asymptotic results yield excellent results for nearly all times of interest. The explicit time-domain fields can be expressed approximately via first-order saddle-point asymptotics as [16]

$$\mathbf{E}(x,y,z,t) \sim \frac{1}{2\pi}\sum_{k=1}^{\infty}\mathbf{e}_k(x,y)d_k(\omega_{sk})\sqrt{\frac{2\pi}{|\phi_k''(\omega_{sk},z,t)|}} \times \exp(j\pi/4)\exp[\phi_k(\omega_{sk},z,t)]. \tag{8}$$

The examples considered below correspond to the case of a rectangular waveguide (Fig. 3), for which the general equations above simplify, yielding further physical insight. In particular, the longitudinal wavenumber for a TE_{mn} or TM_{mn} mode can be expressed as

$$k_{zm0} = \sqrt{k_0^2-(m\pi/a)^2-(n\pi/b)^2} = k_0\cos\theta_{mn}(\omega) \tag{9}$$

where $\theta_{mn}(\omega)$ is the frequency-dependent angle of propagation with respect to the z axis of the rays which constitute the mode. Using (9) in (4) the stationary-point condition becomes

$$\sin\theta_{mn}[\omega_{smn}(z,t)] = \sqrt{1-(z/ct)^2} \tag{10}$$

which indicates that the angle of the wavefront contributing at (z,t) changes with time. The initial wavefronts travel nearly parallel to the z axis ($\theta_{mn} \approx 0$), representing the high-frequency domain of a given mode. As time proceeds, the angle of the wavefront increases with respect to the z axis, and ultimately $\theta_{mn} \to \pi/2$ as $t \gg z/c$ (the cutoff condition). As the angle θ_{mn} increases with time the distance traversed by a wavefront from the input plane at z =0 to the observer at z >0 increases, consistent with the fact that wavefronts that contribute at later portions of the scattered waveform must travel longer distances from the input plane than contributions arriving at earlier times. As demonstrated by Fig. 4, in which for simplicity we consider the special case of TE_{m0} modes (for which the modal rays travel in the x-z plane), (10) further implies that as time proceeds the wavefront seen at the observation point originates from different localized portions of the input field profile.

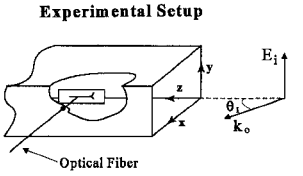

Fig. 3. Schematic of a y-polarized plane wave incident obliquely at angle θ_i to the open end of a rectangular waveguide. Also shown is a representation of how the data in Figs. 10 and 11 were measured. In the measurements a coplanar-strip horn antenna was situated inside the waveguide and optical fiber was fed through a small hole in the side of the waveguide to deliver optical pulses for photoconductive switching [9]–[11].

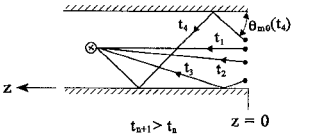

Fig. 4. Physical interpretation of time-domain TE_{m0} propagation in a rectangular waveguide. For this case (10) dictates that $\sin\theta_{m0}[\omega_{sm0}(z,t)] = [1-(z/ct)^2]^{1/2}$, indicating that as time proceeds the angle of wavefronts arriving at the observer increases from an initial angle of $\theta_{m0} \approx 0$ for $t \approx z/c$ to $\theta_{m0} \to \pi/2$ for $t \to \infty$. At any given time the wavefront arriving at a particular time-dependent angle can be back projected to the source plane at $z = 0$, indicating that the wavefronts sample different portions of this plane as time proceeds.

B. Calibration of Asymptotics

The expression in (3) is valid for any hollow waveguide for which the fields $\mathbf{E}(x, y, z = 0, t)$ are known (from which the coefficients $d_k(\omega)$ can be calculated). As an example we consider plane-wave excitation of an open rectangular waveguide, and assume that the aperture transverse electric and magnetic fields at $z = 0$ are the same as the fields of the incident plane wave. Although this is obviously an approximation, it allows us to assess the accuracy of the asymptotics (more-accurate techniques could be used to calculate the aperture fields [17]).

A pulsed plane wave described by the Raleigh wavelet in Fig. 5 is incident obliquely as in Fig. 3. Thus, under our approximation, the aperture fields are polarized in the y direction and only have variation in x, leading to the excitation of TE_{m0} modes. The y-component of electric field E_y can be expressed as

$$E_y = \frac{1}{2a}\sum_{m=1}^{\infty}\int_{-\infty}^{\infty}\frac{mF(\omega)\sin(m\pi x/a)}{(m\pi/a)^2 - k_0^2\sin^2\theta_i} \times [1+(-1)^{m+1}\exp(-jk_0\sin\theta_i a)] \times \exp(j\omega t - j\sqrt{k_0^2-(m\pi/a)^2}z)\,d\omega \quad (11)$$

where $F(\omega)$ is the spectrum of the Raleigh excitation pulse and θ_i is its angle of incidence. For improved accuracy we have found that it is best to break up (11) into the sum of two parts $E_y = E_{y1} + E_{y2}$ where

$$E_{y1} = \frac{1}{2a}\sum_{m=1}^{\infty}\int_{-\infty}^{\infty}\frac{mF(\omega)\sin(m\pi x/a)}{(m\pi/a)^2 - k_0^2\sin^2\theta_i} \times \exp[j\omega t - j\sqrt{k_0^2-(m\pi/a)^2}z]\,d\omega$$

$$E_{y2} = \frac{1}{2a}\sum_{m=1}^{\infty}\int_{-\infty}^{\infty}\frac{mF(\omega)\sin(m\pi x/a)}{(m\pi/a)^2 - k_0^2\sin^2\theta_i}(-1)^{m+1} \times \exp[j\omega t - jk_0\sin\theta_i a - j\sqrt{k_0^2-(m\pi/a^2)}z]\,d\omega. \quad (12)$$

By evaluating E_y in terms of E_{y1} and E_{y2} we can incorporate the phase $\exp(-jk_0\sin\theta_i a)$ into the stationary-point condition, improving the accuracy of the asymptotics. The stationary-point frequency for E_{y1} is

$$\omega_{s1m} = \pm\frac{m\pi}{a}\frac{c^2 t}{\sqrt{(ct)^2 - z^2}}, \qquad t > z/c \quad (13a)$$

and the stationary-point frequency for E_{y2} is

$$\omega_{s2m} = \pm\frac{m\pi}{a}\frac{c^2(t - a\sin\theta_i/c)}{\sqrt{[c(t-a\sin\theta_i/c)]^2 - z^2}}, \qquad t > z/c + a\sin\theta_i/c. \quad (13b)$$

Thus, we see that at any given time E_y is composed of two slightly different frequencies which coalesce with increasing time. The explicit asymptotic expression for E_{y1} is given from (8) to be

$$E_{y1} \sim \frac{1}{2a}\sum_{m=1}^{\infty}\frac{\sin^2\theta_{sm}}{\sin^2\theta_{sm} - \sin^2\theta_i}\frac{cz}{[(ct)^2 - z^2]^{3/4}}\sqrt{\frac{2}{ma}} \times \exp[j\pi/4 - jk_z(\omega_{sm})z + j\omega_{sm}t]F(\omega_{sm}) + \text{c.c} \quad (14)$$

where c.c. represents complex conjugate and

$$\sin\theta_{sm} \equiv \frac{\sqrt{(ct)^2 - z^2}}{ct}. \quad (15)$$

A result similar to that in (14) holds for E_{y2}.

In our example the field E_y is observed $z = 30$ cm from the aperture at $(x = a/2, y = b/2)$, where $a = 1.55$ cm and $b = 1.55$ cm and the angle of incidence is $\theta_i = 45°$. The pulse spectrum and waveguide dimensions have been selected to be consistent with the measurements presented in Section III. We can see from Fig. 6 that the asymptotic approximation in (14) is in close agreement with results calculated via a numerical integration of the spectral integral in (3). The numerical results were computed via a 4096-point fast fourier transform (FFT).

To obtain a better understanding of the waveforms characteristic of each of the time-domain waveguide modes, we plot in Fig. 7 the time-domain TE_{10}, TE_{30}, and TE_{50} modes for the example in Fig. 6 (only modes with even symmetry in x are relevant since the observation point is in the center of the guide). As expected, each time-domain mode is represented by a chirped waveform. It is interesting to note from Fig. 7 that the modal turn-on time appears to increase with increasing modal order (the turn-on time being the approximate time at which a significant amount of energy resides in the form of a particular time-domain mode). This can be explained by Fig. 8 in which we have plotted the incident-pulse spectrum and the time-dependent dispersion curves in (13a) and (13b). We see that as the modal cutoff frequency increases (with increasing modal order), there is an increase in the time at which the time-dependent dispersion curves begin to reside within the input-pulse spectrum.

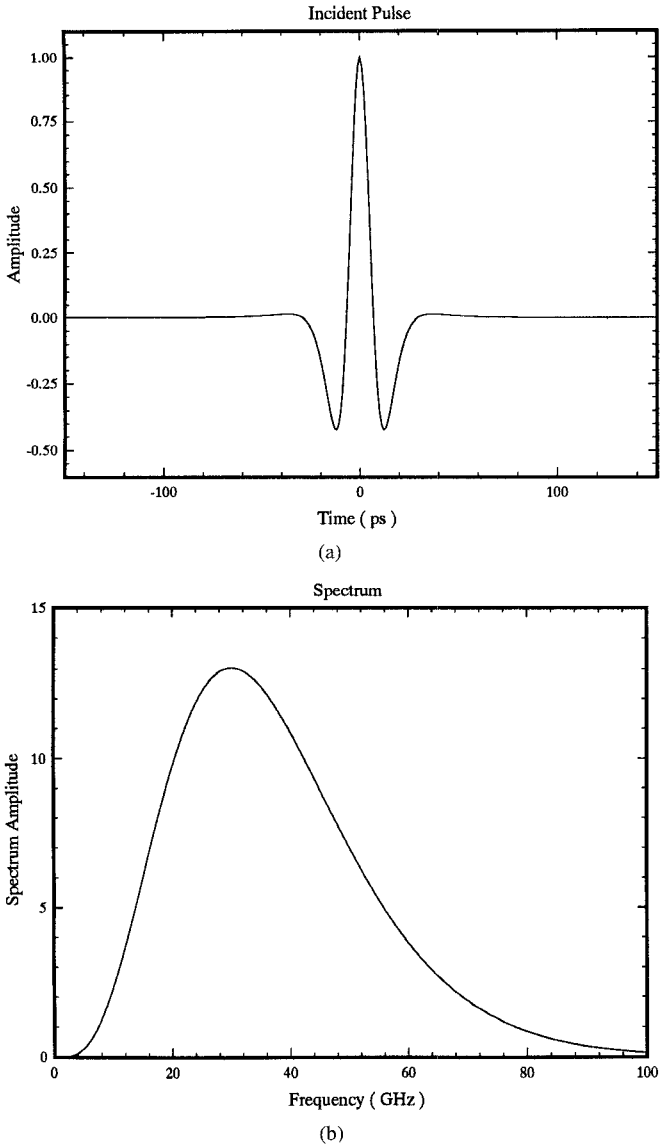

Fig. 5. Pulse shape and spectrum for the Raleigh wavelet [18] used as the incident waveform in our calculations. (a) Time-domain pulse, (b) spectrum.

III. Experimental Results and Time-Frequency Processing

To demonstrate this phenomenology experimentally we have performed optoelectronic measurements in which freely propagating short-pulse radiation is generated by switching planar antennas photoconductively. We use coplanar-strip horn antennas fabricated on oxygen-bombarded silicon-on-sapphire wafers. The optical pulses are generated by a mode-locked CW Nd-YLF laser which is pulse compressed and frequency doubled to produce approximately 4 ps duration green pulses (λ =527 nm) at a 76 MHz repetition rate and 150 mW average power. The optical pulses are split into pump and probe beams, with each beam subsequently coupled into single-mode optical fiber. The optical-fiber fed pump beam is used to switch a dc-biased antenna, generating a freely propagating burst of radiation with instantaneous bandwidth from 15–75 GHz; the probe beam is time delayed with respect to the pump beam and is used to time gate the waveform on the receive antenna,

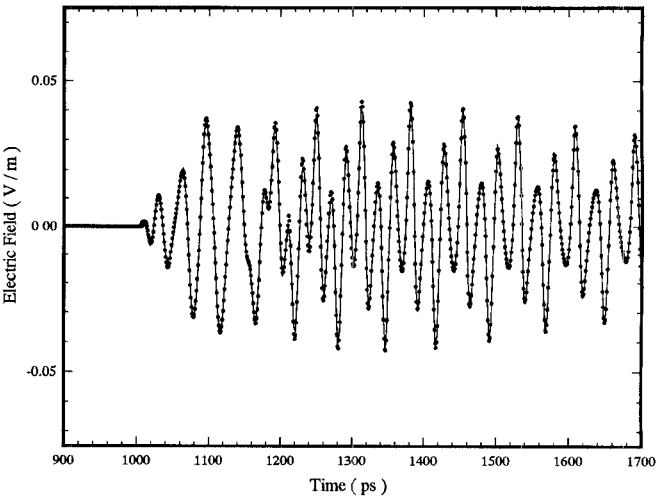

Fig. 6. Calculated time-domain fields observed 30 cm from the open end of a rectangular due to pulsed plane-wave excitation as in Fig. 3 ($\theta_i = 45°$). The incident pulse shape is described in Fig. 5 and the waveguide dimensions are $a = 1.55$ cm and $b = 1.55$ cm. The solid curve represents the results of an FFT of (11) while the points were calculated by the asymptotic expression in (14).

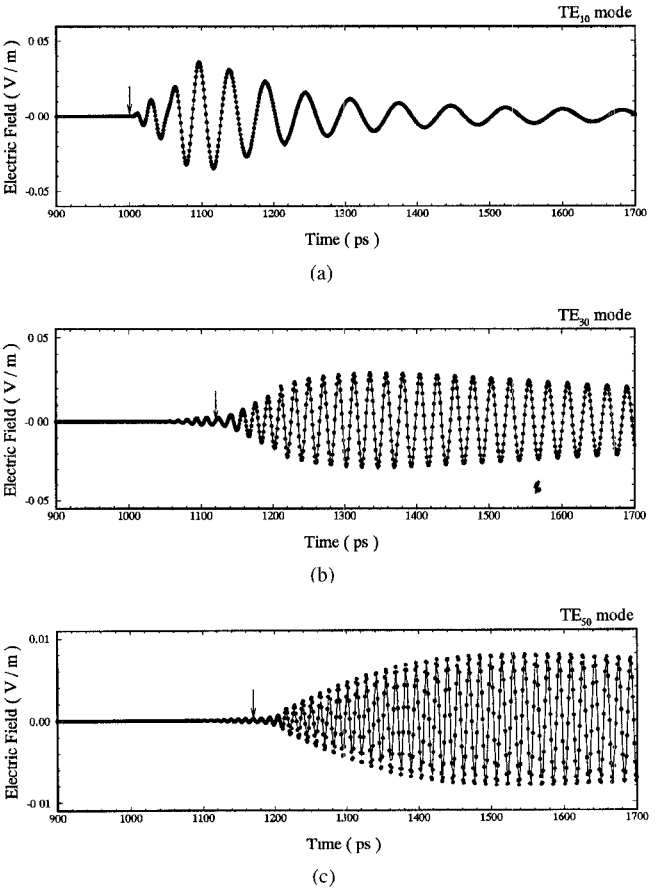

Fig. 7. Time-domain fields for the TE_{10}, TE_{30} and TE_{50} modes for the geometrical parameters and excitation pulse considered in Fig. 6. The solid curve represents the results of an FFT of (11) while the points were calculated by the asymptotic expression in (14). Indicated by arrows are the approximate modal turn-on times as given by Fig. 8. (a) TE_{10}, (b) TE_{30} and (c) TE_{50}.

its optical path length being adjusted by mirrors placed on a precision computer-controlled translational stage. The time-

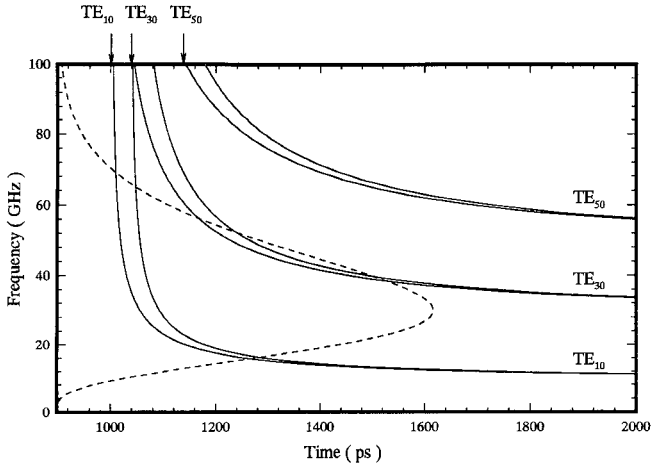

Fig. 8. Time-dependent modal dispersion curves described in (13a) and (13b) for time-domain TE_{m0} modes in a rectangular waveguide; the physical parameters are as considered in Figs. 6 and 7. Shown dashed is the pulse spectrum of the incident waveform, with amplitude units as described in Fig. 5 The arrows indicate the approximate times at which the respective time-dependent modal dispersion curves first reside within the excitation-pulse spectrum, identifying the approximate modal turn-on time; these arrows are also displayed in Fig. 7.

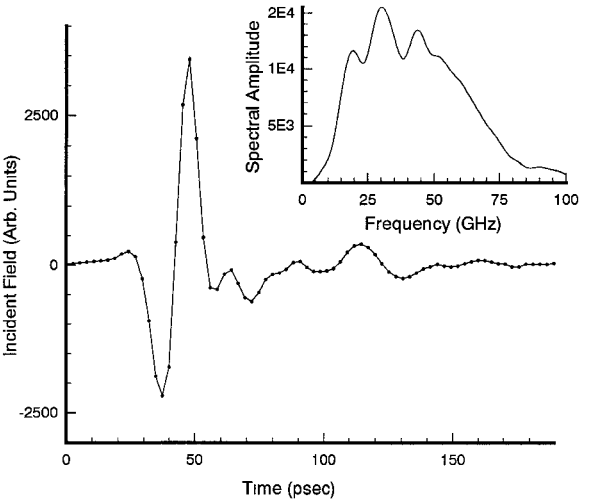

Fig. 9. Typical reference pulse and its spectrum, measured in the absence of the waveguide.

gated waveform on the receive antenna is averaged by a lock-in amplifier. Details about the experimental facility are given in [9]–[11].

A. Pulsed-Beam Excitation

In our first set of measurements the pulsed radiation was collimated using a fused-silica hemispherical lens, generating a pulsed beam with approximately linear polarization. These fields were made incident at $\theta_i = 45°$ on the open end of a rectangular waveguide with $a = 1.55$ cm and $b = 1.55$ cm, and the electric field was polarized parallel to the y axis (see Fig. 3). We have demonstrated previously that the beam is approximately uniform over a 3 cm diameter and therefore for this incident polarization we anticipate that only TE_{m0} modes will be excited (no variation in the y direction). The fields were measured by placing a second coplanar-strip horn antenna inside the waveguide (Fig. 3) and drilling a small hole in the side of the waveguide through which the probe beam was directed via optical fiber. Due to the small diameter of the optical fiber (radius of 0.25 mm), the hole in the side of the waveguide and the fiber itself introduced negligible perturbation to the waveguide fields. The coplanar-strip transmission-line antenna feed consisted of 20 μm wide lines with 10 μm interstrip spacing; in the horn region the maximum separation between the outermost edges of the two lines was less than 4 mm. Thus the antenna itself also introduced only a minor perturbation of the fields inside the waveguide. The waveguide extended in back of the probe antenna for a sufficient distance such that no reflections from the end of the waveguide were present in the measurement time window.

The incident pulse and spectrum are shown in Fig. 9 (measured in the absence of the waveguide) and the results of the waveguide measurement are demonstrated in Fig. 10. As discussed above, the co-planar-strip horn antenna has been shown previously to be approximately linearly polarized, and for the measurements in Fig. 10 the receiving antenna was oriented such that E_y was measured. The results in Fig. 10 are presented as follows: the bottom plot represents the measured fields E_y with the probe antenna placed in the center of the waveguide $z = 4.7$ cm from the open end, the left plot represents a numerical Fourier transform of the entire measured waveform, and the center plot represents the results of a short-time Fourier transform (STFT) using a Gaussian window with a 90 ps 3 dB width. In the time-frequency phase space (center) are also plotted the time-dependent dispersion curves given by (13a) and (13b) for the TE_{10}, TE_{30}, and TE_{50} modes. The results of the STFT—which demonstrate the time-frequency behavior of the time-dependent waveguide modes—are in close agreement with the predictions in (13a) and (13b); however, due to the pulse bandwidth only the TE_{10} and TE_{30} modes are excited strongly, while the TE_{50} mode is excited much more weakly. Note that as time proceeds the frequency content of the TE_{10} mode approaches 10 GHz, and from Fig. 9 it is seen that the incident pulse has little energy around this frequency. Thus, at early times mode TE_{10} is excited strongly but as time proceeds its excited strength diminishes as its instantaneous frequency lowers and moves below the spectrum of the incident pulse. At late times the fields are represented almost entirely by the TE_{30} mode.

A comment should be made with regard to the results in Fig. 10. When performing a pump-probe optoelectronic measurement, one actually measures a convolution of the actual fields (E_y in this example) with the impulse response of the photoconductive detection system. However, by examining the time-frequency results of Fig. 10, which are in good agreement with the expectations of (13a) and (13b), we see that the impulse response of the detector does not appear to corrupt the time-frequency distribution of E_y significantly. To further substantiate this point, we de-embedded the response of the detector by dividing the Fourier transform of the waveform at the bottom of Fig. 10 by the Fourier transform of a reference pulse (such as the one in Fig. 9), yielding the impulse response of the system $H(\omega)$ over the system bandwidth. A new time-

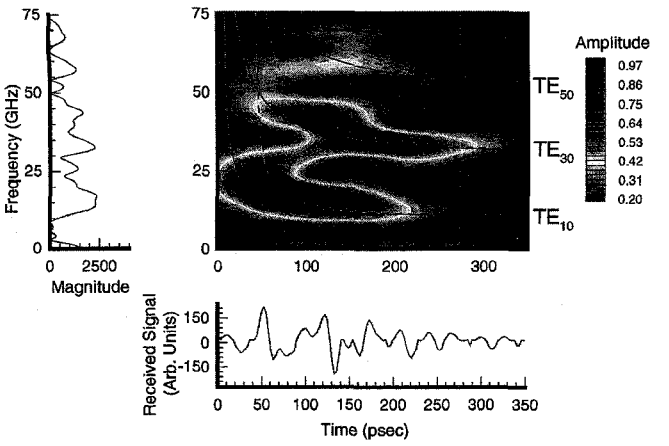

Fig. 10. Measured time-domain waveform (bottom), numerical Fourier transform (left), and short-time Fourier transform (center) for the structure considered in Fig. 5. The field E_y was measured in the center of the waveguide $z = 4.7$ cm from the open end, with $\theta_i = 45°$ and $a = b = 1.55$ cm. Also shown are the predicted time-dependent dispersion curves for the TE_{10}, TE_{30} and TE_{50} modes using (13a) (solid) and (13b) (dashed).

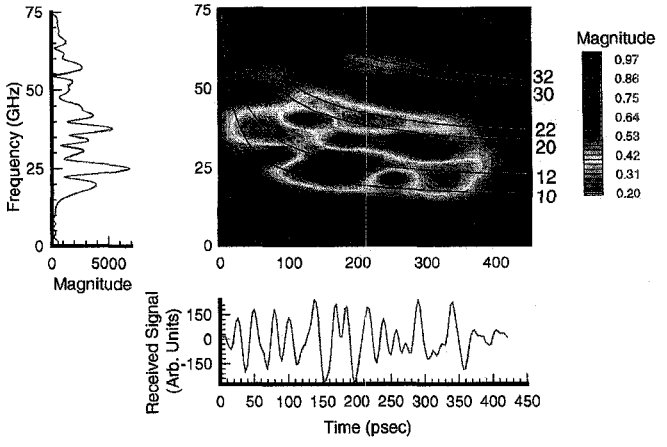

Fig. 11. Measured time-domain waveform (bottom), numerical Fourier transform (left), and short-time Fourier transform (center) for the receive antenna placed as in Fig. 5 but with the transmitting antenna placed inside the waveguide $z = 10.7$ cm from the detector. Waveguide dimensions: $a = 1$ cm and $b = 2.2$ cm, location of receive antenna: $(x = a/5, y = b/2)$, and location of transmitting antenna: $(x = a/2, y = b/2)$. Also plotted are the time-dependent dispersion curves predicted from (13a) for TE_{mn} and TM_{mn} modes (m and n are labeled on the right side of the center plot).

domain signal for the waveguide problem was calculated by multiplying $H(\omega)$ by the spectrum of a synthetic pulse with bandwidth consistent with our measurement. After repeating the STFT processing in Fig. 10 on the synthesized waveform, we observed no appreciable change in the time-frequency phase space.

B. Localized-Source Excitation

Our second series of measurements were conducted with both the transmitting and receiving antennas placed inside a rectangular waveguide with $a = 1$ cm and $b = 2.2$ cm. For these measurements no lens was used on the transmitting antenna, and therefore it represented a localized source of pulsed radiation. The transmitting antenna was placed in the center of the waveguide cross section, with its metallization parallel to the (y, z) plane. The receiving antenna was positioned at $x = a/5$ and $y = b/2$, a longitudinal distance 10.7 cm from the transmitter; the receiving antenna was so positioned such that we could measure modes for which E_y has odd symmetry in x. The results for this example are presented in Fig. 11 using the same format as in Fig. 10. In Fig. 11 we have also plotted the instantaneous dispersion curves from (13a) [(13b) results from the assumption of plane-wave excitation, which is not considered here]; note that the TE_{mn} and TM_{mn} modes have the same dispersion relations for like (m, n) and therefore the dispersion curves alone cannot distinguish the TE and TM modes. For both TE_{mn} and TM_{mn} modes E_y has a $\sin(m\pi x/a)\cos(n\pi y/b)$ transverse variation; because the receiving antenna is centered in the y direction and off center in the x direction $m \in [1, 2, 3, \ldots)$ and $n \in [0, 2, 4, \ldots)$.

In STFT time-frequency processing one uses a fixed-size window function which is slid across the time-domain data. At each window position a Fourier transform is taken, providing information about the waveform's time-dependent frequency content. The frequency resolution is dictated by the size of the time-domain window (in Fig. 11 we have used a Gaussian window with a 90 psec wide 3 dB point). Therefore one must compromise between temporal localization and frequency resolution. In Fig. 11 the frequency resolution is inadequate to distinguish between the $(m, n = 0)$ and $(m, n = 2)$ modes, where m =1, 2, and 3 (in the vicinity of 210–290 ps, however, the (1, 0) and (1, 2) modes appear to be discernable). To obtain better frequency resolution one must increase the window size, with the inevitable loss of temporal resolution. The window size used for Fig. 11 yielded the best compromise between temporal localization and frequency resolution and provided the best agreement with the time-domain dispersion curves predicted in (13a).

IV. Conclusion

An asymptotic analysis has been performed for short-pulse propagation in a hollow waveguide. The asymptotic results demonstrate that time-domain waveguide modes are characterized by time-dependent instantaneous frequencies which are large at early times and decrease to the modal cutoff frequency with increasing time. The asymptotic parametrization of the time-domain fields in terms of chirped waveguide modes applies to waveguides of arbitrary cross section, but has been examined here numerically and experimentally for the case of rectangular waveguide. In our numerical example of a pulsed plane wave incident on the open end of a rectangular waveguide, the frequency domain waveguide modes were converted to the time domain asymptotically as well as via a fast Fourier transform (FFT). Except for very early times, the asymptotic data were in nearly exact agreement with the results of the FFT. Moreover, the asymptotic analysis was also capable of predicting the approximate modal turn-on times. The measurements were performed optoelectronically using a short-pulse laser to switch planar antennas photoconductively, generating freely propagating bursts of radiation with instantaneous bandwidth from 15–75 GHz. The first experiment considered pulsed radiation incident obliquely upon the open end of a rectangular waveguide, while the second considered

a pulsed antenna placed inside the waveguide; in both cases the fields were measured optoelectronically using an antenna situated inside the guide. The measured time-domain fields were processed using a short-time Fourier transform, and the time-frequency results were found to be in good agreement with the predictions of the asymptotic analysis.

ACKNOWLEDGMENT

The last author wishes to thank Prof. L. B. Felsen of Boston University for several stimulating discussions on high-frequency asymptotics and time-domain structural dispersion.

REFERENCES

[1] L. Brillouin, *Wave Propagation and Group Velocity*. New York: Academic, 1960.
[2] J. D. Jackson, *Classical Electrodynamic*. ch. 7, 2nd ed., New York: Wiley, 1975.
[3] K. E Oughstun, J. E. K. Laurens, and C. M. Balictsis, "Asymptotic description of electromagnetic pulse propagation in a linear dispersive medium," in *Ultra-Wideband, Short-Pulse Electromagnetics*. H. L. Bertoni, L. Carin, and L. B. Felsen, Eds. New York: Plenum, 1993, pp. 223–240.
[4] L. Carin and L. B. Felsen, "Time-harmonic and transient scattering by finite periodic flat strip arrays: Hybrid (Ray)-(Floquet Mode)-(MOM) algorithm and its GTD interpretation," *IEEE Trans. Antennas Propagat.*, vol. 41, pp. 412–421, Apr. 1993.
[5] L. B. Felsen and L. Carin, "Diffraction theory of frequency- and time-domain scattering by weakly aperiodic truncated thin-wire gratings," *J. Opt. Soc. Am. A*, vol. 11, pp. 1291–1306, Apr. 1994.
[6] F. Niu and L. B. Felsen, "Time-domain leaky modes on layered media: Dispersion characteristics and synthesis of pulsed radiation," *IEEE Trans. Antennas Propagat.*, vol. 41, pp. 755–761, June 1993.
[7] W. Su, I. M. Besieris, and S. M. Riad, "Velocity of an RF pulse signal propagating in a waveguide," *IEEE Microwave and Guided Wave Lett.*, vol. 2, pp. 255–256, June 1992.
[8] P. Stenius and B. York, "On the propagation of transients in waveguide," *IEEE Antennas Propagat. Mag.*, June 1995.
[9] G. Arjavalingam, Y. Pastol, J.-M. Halbout, and G. V. Kopcsay, "Broadband microwave measurements with transient radiation from optoelectronically pulsed antennas," *IEEE Trans. Microwave Theory Tech.*, vol. 38, pp. 615–621, May 1990.
[10] D. Kralj and L. Carin, "Short-pulse scattering measurements from dielectric spheres using optoelectronically switched antennas," *Appl. Phys. Lett.*, vol. 62, pp. 1301–1303, Mar. 15, 1993.
[11] A. Rahman, D. R. Kralj, and L. Carin, "Photoconductively switched antennas for measuring target resonances," *Appl. Phys. Lett.*, vol. 64, pp. 2178–2180, Apr. 1994.
[12] L. Cohen, "Time-frequency distributions—A review," *Proc. IEEE*, vol. 77, pp. 941–981, July 1989.
[13] A. Moghaddar and E. K. Walton, "Time-frequency distribution analysis of scattering from waveguide cavities," *IEEE Trans. Antennas Propagat.*, vol. 41, pp. 677–679, May 1993.
[14] L. Carin and L. B. Felsen, "Wave-oriented data processing for frequency and time domain scattering by nonuniform truncated array," *IEEE Antennas Propagat. Mag.*, June 1994.
[15] N. Marcuvitz, *Waveguide Handbook*. London: Peregrinus, 1986.
[16] L. B. Felsen and N. Marcuvitz, *Radiation and Scattering of Waves*. Englewood Cliffs, NJ: Prentice-Hall, 1973.
[17] H. Ling, S.-W. Lee, and R.-C. Chou, "High-frequency RCS of open cavities with rectangular and circular cross sections," *IEEE Trans. Antennas Propagat.*, vol. 37, pp. 648–654, May 1989.
[18] P. Hubral and M. Tygel, "Analysis of the Raleigh pulse," *Geophysics*, vol. 54, pp. 654–658, 1989.

David Kralj was born May 14, 1968 in Mar del Plata, Argentina. He became a United States citizen in 1992. He received the B.S. and M.S. degrees in electrical engineering from Polytechnic University, Brooklyn, NY in 1993 and 1995, respectively. He is currently pursuing the Ph.D. degree at the same university.

His research interests include optoelectronics and electromagnetics.

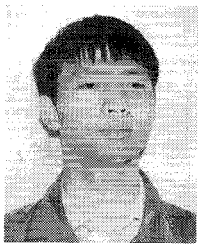

Lin Mei was born April 1974 in Luoyang, China. He is currently an undergraduate student at Polytechnic University, pursuing a bachelor's degree in electrical engineering.

He was a first prize winner in China's Eighth National High School Physics competition in 1990. During 1994, he was a NSF Summer Research Assistant at Polytechnic University.

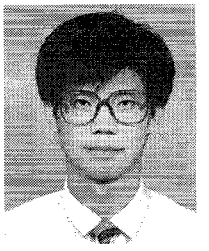

Teng-Tai Hsu (S'90-M'95) was born in Chiayi, Taiwan on May 20, 1963. He received the B.S. degree in electrical engineering from National Taiwan University, Taipei, Taiwan, in 1985, the M.S. degree in electronics engineering from National Chiao-Tung University, Hsinchu, Taiwan, in 1990, and the Ph.D. degree in electrical engineering from Polytechnic University, Brooklyn, New York, in 1995.

His research areas are numerical and theoretical methods in electromagnetics and signal processing in wave-oriented problems.

Dr. Hsu is a member of Eta Kappa Nu and Tau Beta Pi.

Lawrence Carin (S'86–M'89), for a photograph and biography, see this issue, p. 2072.